I&EC research
Industrial & Engineering Chemistry Research

pubs.acs.org/IECR
Article

Effect of Copper Catalyst Content and Zinc Promoter on Carbon Formation in the Direct Synthesis of Methylchlorosilanes

Published as part of Industrial & Engineering Chemistry Research virtual special issue "Dmitry Murzin Festschrift".

Mehdi Mahmoodinia, Hammad Farooq, Torbjørn Røe, Ingeborg-Helene Svenum, and Hilde J. Venvik*

Cite This: *Ind. Eng. Chem. Res.* 2023, 62, 21579−21589

ABSTRACT: Direct synthesis of methylchlorosilanes (MCS) is a complex solid−gas−solid reaction where solid silicon (Si) reacts with chloromethane (CH_3Cl) in the presence of a copper (Cu)-based catalyst, and coke formation by cracking of CH_3Cl is a severe problem for this process. In this study, the effects of the Cu/Si ratio and Zn promoter on the MCS catalytic performance have been investigated in a fluidized bed lab-scale reactor (semibatch mode). Pre- and postcharacterization (SEM, XRD, Raman and DRIFTS spectroscopy, and TGA/DCS/MS) were performed to gain insights into the structure and reactivity of the carbonaceous species, the formation of active (Cu_3Si) and unselective/coke-promoting (Cu_xSi_y, Cu^0) phases. A higher content of the CuCl catalyst (5 × Cu) boosts the Si consumption and initial reactivity with little effect on dimethyldichlorosilane ($(CH_3)_2SiCl_2$; "M2") selectivity other than a slightly longer induction period relative to the standard Cu/Si ratio, but it also promotes formation of undesired phases and hence coke. The effect of Zn promotion (in conjunction with Sn) is difficult to discern with standard amounts of CuCl and Zn added to the contact mass, but with increased amounts, Zn clearly facilitates the formation of the active catalytic phase and also appears to render the amorphous carbonaceous species formed somewhat more structurally ordered and H-depleted. The work expands our understanding of the MCS synthesis since both the Cu/Si ratio and Zn promotion affect the mechanisms as well as the propensity to form coke.

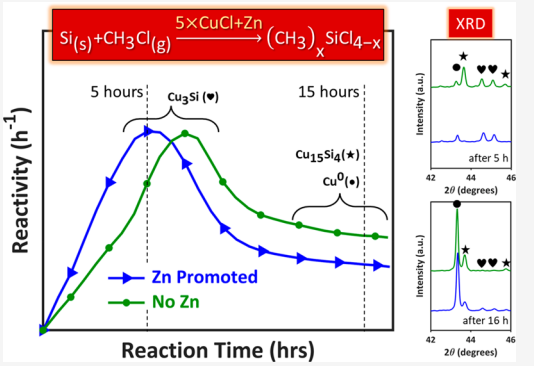

1. INTRODUCTION

The reaction between chloromethane (CH_3Cl, also called methyl chloride) and silicon (Si) to synthesize methylchlorosilanes (MCS), also known as the Müller-Rochow Synthesis or the Direct Process, is currently the most convenient and economical way to produce MCS industrially. Almost 90% of the starting materials for current silicone manufacturing are obtained with MCS monomers.[1−3] On an industrial scale, ground metallurgical grade silicon is mixed with a copper-based catalyst[4−9] and minor amounts of various other promoter elements[10−15] in a fluidized bed reactor under gaseous CH_3Cl, at temperature and pressure ranging between 280−350 °C and 1−10 bar.[11,16] This quite unique gas (CH_3Cl)−solid (Si)−solid (Cu-based catalyst) heterogeneous reaction exhibits a complicated dependency on reaction temperature, (partial) pressure(s), reactor type, residence time distribution, and phase/component interactions.[5,11] The latter incorporates nature, purity, size distribution, morphology, and proportion of silicon to copper catalyst precursor and promoters.[17] Moreover, a range of methylchlorosilanes, $(CH_3)_xSiCl_{4-x}$, is formed although the dominant and main product of interest is dimethyldichlorosilane, $(CH_3)_2SiCl_2$, also referred to as "M2".[18] Other side products formed during the direct process include hydrocarbons and high- and low-boiling Si-containing residues.[1]

Discussions on the detailed mechanism of the MCS reaction and the role of copper as the main catalyst have a long history.[19] Unlike typical heterogeneous catalytic processes, the solid phase reactant (Si) must first interact with the Cu-based catalyst precursors to form a contact mass containing copper-silicide phases. It has previously been reported that Cu_3Si, also referred to as η-phase, acts as the most active catalytic phase.[20] Si is thus not only a reactant but also part of the catalytically active phase.[21] The broad product distribution and the small impurities in the metallurgical grade silicon (i.e., Fe, Al, Ca, etc.) add to the complexity.[1,19,22,23] Several Cu-based

Received: August 25, 2023
Revised: November 5, 2023
Accepted: November 13, 2023
Published: December 9, 2023

compounds such as CuO, Cu_2O, CuCl, and also combinations thereof have been used as the catalyst precursors in the MCS synthesis.[4−9] CuCl is regarded as efficient in this respect, since it not only reduces the induction period but also increases the selectivity toward M2.[5] Several other metals are reported to enhance the catalytic activity, selectivity, and stability of copper in the direct process.[10−15] For example, there is a general agreement in the literature that zinc (Zn) increases the selectivity toward M2,[10,14] and that its copromotion with tin (Sn) results in a synergistic relationship that increases both reaction rate and M2 selectivity.[12,24]

Adsorption and decomposition of CH_3Cl on the surface into CH_3* and Cl* (* indicates adsorbed species) are an initial assumption for the primary MCS reaction.[25] Further decomposition of the CH_3* group is commonly referred to as "cracking". During the MCS process, several silicon-free products are also formed through catalytic and/or thermal cracking of CH_3Cl.[26−28] These products include volatile molecules, such as methane, ethane, ethylene, hydrogen, hydrogen chloride, and certain higher hydrocarbons, as well as nonvolatile carbonaceous material (also referred to as "coke"). The latter deposits on the contact mass and results in deactivation of active phases, which causes operational, economic, and environmental problems. Several mechanisms have been proposed for coke formation. Bažant proposed that the coke is mainly comprised of polymethylenes, formed via dehydrogenation of CH_3* to CH_2*, CH*, and C* species, and a recombination of these.[27] Clarke claimed that coke is mainly formed from CH_3Cl cracking on copper, e.g., $2Cu + 2CH_3Cl \rightarrow 2CuCl + CH_4 + H_2 + C$.[29] Wessel et al. reported an enhanced coke deposition at higher reaction temperatures.[30] It has also been reported that insufficient fluidization in the reactor may lead to the formation of localized hot spots,[31] up to 1000 °C during the industrial direct synthesis, thereby facilitating thermal cracking of CH_3Cl. The deposited coke may contain chlorine, in which case it has been found to further catalyze the cracking process at lower temperatures, i.e. an autocatalytic effect.[32]

Although significant progress has been made over 70 years, the actual carbon formation mechanism and the nature of the carbon formed remain to be understood to the extent that it enables inhibition or a high degree of predictability in industrial operation. The amount and nature of carbon species are affected by the reaction conditions, type of catalyst precursor, selection of promoters, and reactor type, and it would be beneficial to learn more about the initiation of cracking to learn how to suppress it. In the present study, a series of contact mass samples with varying ratios of CuCl to Si contents and addition of Zn and Sn as promoters were therefore prepared and tested in a fluidized bed semibatch lab reactor for the MCS process with relatively short reaction times. To evaluate the effect of relative CuCl concentration and role of Zn on the catalytic performance, the coke formation, and the Cu_xSi_y phase transformations, we have investigated the crystalline structure, morphological properties, and the surface chemical features of the reacted contact mass samples. Furthermore, a qualitative approach is taken to characterize the thermal and structural properties of the deposited coke. This provides additional insight into the cracking mechanism and coke deposition on the contact mass particles.

2. MATERIALS AND METHODS

2.1. Sample Preparation. Five grams of metallurgical grade silicon (Si 99 wt %, Fe < 0.4 wt %, Al < 0.4 wt %, Ca < 0.1 wt %, produced by Elkem Thamshavn), milled and sieved to 71−125 μm, was mixed with a catalyst and promoters for the contact mass samples. The amount of catalyst (high purity CuCl) was either standard for our laboratory experiments (termed std-Cu), or elevated (termed 5 × Cu) to provoke the effect of increased amounts of CuCl in the initial contact mass, or alternatively, a high degree of Si consumption without the other effects of a progressed reaction, e.g. coke, present. The contact mass samples were either with or without Zn to study the role of this promoter, while Sn was always added as a promoter. The details of sample composition are summarized in Table 1. The "standard" samples correspond to 97.5 wt % Si and 2.5 wt % of CuSnZn, while those with 5 × Cu consist of 87.5 wt % Si and 12.5 wt % of CuZnSn. The exact Zn and Sn (ppm quantities) amounts are proprietary, something that also applies to other (low level) impurities in the metallurgical grade Si. The amounts of promoters (Zn and Sn) were, however, increased by only 3 times in the 5 × Cu samples to limit unrealistic effects from these elements.

2.2. Catalytic Performance. Evaluation of the catalytic performance of the contact mass mixtures was carried out in a fluidized bed lab-scale reactor. The samples were reacted with a continuous flow of 285 NmL/min CH_3Cl gas in a semibatch mode (i.e., with no subsequent addition of contact mass) at near-ambient pressure and 300 °C (reactor wall temperature). Argon gas (10 NmL/min) was cofed continuously as an internal standard. The effluent gas composition, comprising Si-based gaseous products (i.e., M1: CH_3SiCl_3, M2: $(CH_3)_2SiCl_2$, M3: $(CH_3)_3SiCl$, MH: CH_3SiHCl_2, M2H: $(CH_3)_2SiCl$, $(CH_3)_3Si_2Cl_3$, and $(CH_3)_4Si_2Cl_2$), was quantified by gas chromatography using a Varian 3800 Gas Chromatograph equipped with a packed column and a TCD detector.

The reaction experiments were carried out for set time periods of 5 and 16 h, which are intended to yield information regarding the initial phase of an industrial run. At the end of the experimental run, samples of reactor residue contact mass were transferred (under argon) from the reactor to a small, sealed glass bottle with a screw cap. The bottles were stored in a glovebox under N_2 before being transferred to the different characterization apparatuses.

Silicon consumption, reactivity, and selectivity toward, e.g., M2 is calculated as follows:

Table 1. List of Analyzed Contact Mass Samples[a]

Samples/description	Promoters	Run time (h)
Pure CuCl	-	-
Si-Ref − Metallurgical grade Si	-	-
S0 − 97.5%Si2.5%CuZnSn	Sn, Zn	0
S1 − 97.5%Si2.5%CuZnSn−5 h	Sn, Zn	5
S2 − 97.5%Si2.5%CuSn−5 h	Sn	5
S3 − 97.5%Si2.5%CuZnSn−16 h	Sn, Zn	16
S4 − 97.5%Si2.5%CuSn−16 h	Sn	16
S5 − 87.5%Si12.5%CuZnSn−5 h	Sn, Zn*	5
S6 − 87.5%Si12.5%CuSn−5 h	Sn*	5
S7 − 87.5%Si12.5%CuZnSn−16 h	Sn, Zn*	16
S8 − 87.5%Si12.5%CuSn−16 h	Sn*	16

[a]Note that Sn and Zn were only increased ×3, while CuCl was increased ×5.

https://doi.org/10.1021/acs.iecr.3c02940
Ind. Eng. Chem. Res. 2023, 62, 21579−21589

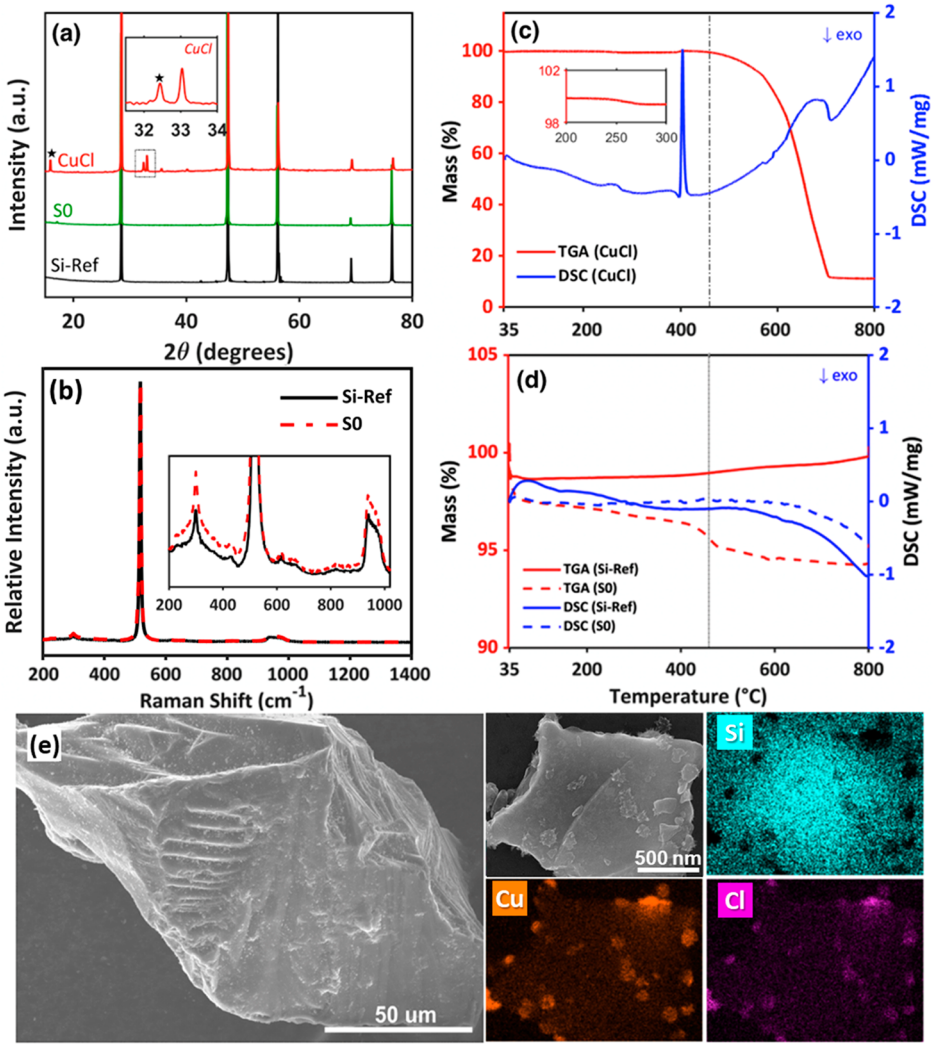

Figure 1. Characteristics of catalyst (CuCl), metallurgical grade silicon (Si-Ref), and unreacted contact mass (S0). (a) XRD patterns, offset along the *y*-axis for clarity, ★ symbol refers to $CuCl_2$ (impurity); (b) Raman spectra, normalized to the main peak (519 cm^{-1}) with the inset displaying intensity differences; (c) CuCl and (d) Si-Ref and S0 TGA/DSC profiles with dashed vertical lines indicating the melting point of CuCl (422 °C); (e) SEM mages and elemental mapping of S0.

$$\text{Si Consumption}\ (\%) = \frac{m_{\text{Si},0} - m_{\text{Si},t}}{m_{\text{Si},0}} \times 100 \quad (1)$$

$$\textit{Reactivity}\ (h^{-1}) = \frac{\sum \dot{m}_{\text{M}i}}{m_{\text{Si},t}} \quad (2)$$

$$\text{M2}\ \textit{Selectivity}\ (\%) = \frac{\dot{m}_{\text{M2}}}{\sum \dot{m}_{\text{M}i}} \times 100 \quad (3)$$

Here, $m_{\text{Si},0}$ and $m_{\text{Si},t}$ represent the Si mass in the reactor at the start and at reaction time t, respectively, with $m_{\text{Si},t}$ calculated from the integrated formation of Si containing products. $\dot{m}_{\text{M2}}$ is the mass flow rate of dimethyldichlorosilane in the product stream. $\dot{m}_{\text{M}i}$ refers to the mass flow of gaseous product i.

2.3. Characterization. X-ray diffraction (XRD) analysis was performed on a Bruker D8 A25 DaVinci X-ray Diffractometerusing Cu−Kα radiation (λ = 1.54060 Å), in continuous scan mode where a step size of 0.014°, time step of 0.4 s, and fixed divergence slit of 0.3° were used. The diffraction patterns were matched with the ICDD PDF-4+ database to identify the crystalline phases present. Morphological and elemental analyses of the near-surface region were made by scanning electron microscopy (SEM) using a Hitachi SU9000 S(T)EM instrument coupled to the Oxford Ultim Extreme EDX-system. Raman spectra were obtained using a Horiba Jobin Yvon LabRAM HR800 spectrometer, utilizing a 633 nm He−Ne laser excitation source at 8 mW power and a 50× objective lens. Diffuse reflectance infrared Fourier transform spectroscopy (DRIFTS) was performed on a Bruker Vertex 80v IR-Spectrometer. Thermogravimetric analysis (TGA), differential scanning calorimetry (DSC), and mass spectrometry (MS) analyses were obtained using a Netzsch STA 449C Jupiter TGA/DSC coupled with a Netzsch Aëolos QMS 403C. The samples were heated to 800 °C (from 35 °C at 10 °C/min) under 25 mL/min Ar (protective gas) and 55 mL/min synthetic air.

3. RESULTS

3.1. Characterization of Si, CuCl, and Unreacted Contact Mass. The physical and chemical characteristics representative of samples before undergoing any reaction, i.e., metallurgical grade silicon (Si-Ref), unreacted contact mass (S0), and CuCl, are presented in Figure 1. The X-ray diffractograms (Figure 1a) of Si-Ref and CuCl display the

https://doi.org/10.1021/acs.iecr.3c02940
Ind. Eng. Chem. Res. 2023, 62, 21579−21589

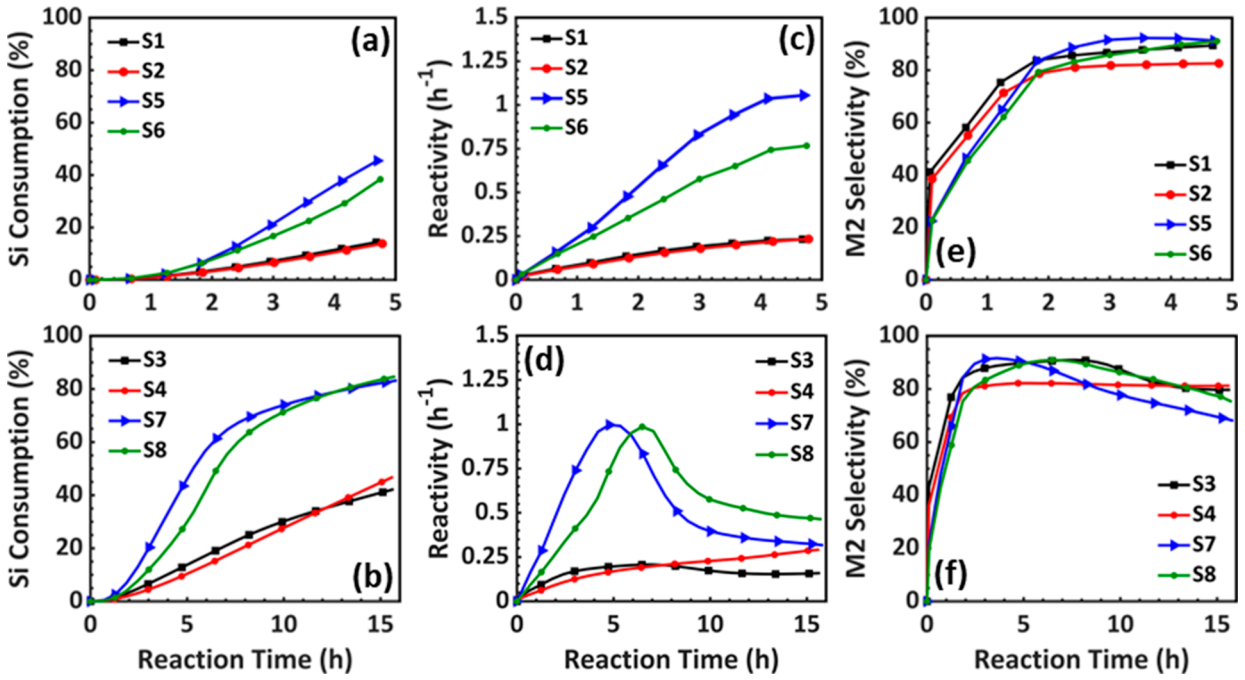

Figure 2. Evaluation of catalytic performance of CuCl in various contact mass samples at 300 °C; (a−b) Silicon consumption, (c−d) Reactivity toward M*i* (mass of MCS products per mass of unreacted silicon per hour), and (e−f) M2 Selectivity (mass fraction of $(CH_3)_2SiCl_2$ in the gaseous product effluent). S1−4: std-Cu; S5−8: 5 × Cu; S1, 3, 5, 7: Zn promoted; S2, 4, 6, 8: no Zn (all samples Sn promoted).

characteristic peaks of bulk silicon (ICDD PDF#00-005-0565) and CuCl (ICDD PDF#04-007-2951), respectively. The diffraction pattern of CuCl overlaps with that of silicon to a large extent, except for a relatively weak peak at a 2θ value of 33.0°, which is not detected in the diffractogram of S0.[33] The standard amount of catalyst (2.5 wt %) is thus insufficient with respect to capturing the presence of CuCl in unreacted contact mass. This must be considered when interpreting the XRD results from the reacted mass samples. The small peaks near 16.0° and 32.5° in the diffractogram from CuCl belong to $CuCl_2$(impurity).[34] Likewise, these peaks could not be detected in the unreacted contact mass sample (S0).

Raman spectra for Si-Ref and S0 are displayed in Figure 1b. The major bands at Raman shift values of 300, 430, 519, 615, and 940 cm^{-1} in both samples belong to phononic modes unique to silicon.[35] The bands around 300, 615, and 940 cm^{-1} all show a higher intensity in the unreacted contact mass (S0). Copper oxide species exhibit Raman bands at around 293 and 623 cm^{-1},[36] but the increase also at 940 cm^{-1} suggests this difference is due to experimental imprecision. Overall, the two samples appear similar, dominated by Si.

The TGA and DSC results obtained under an oxidative atmosphere for CuCl, Si-Ref, and S0 are plotted in Figure 1c-d. The CuCl sample displays insignificant mass loss below 100 °C due to drying and a small but continuous mass loss up to 300 °C (inset plot in Figure 1c). The latter might be due to moderate oxidation of CuCl.[37] The sharp endothermic DSC signal peak (Figure 1c) signifies the CuCl melting point at 423 °C.[37] Thereafter, the sample experiences almost an 88% mass loss. CuCl decomposes and vaporizes as $Cu_3Cl_{3(g)}$, $Cu_4Cl_{4(g)}$, and $Cu_5Cl_{5(g)}$ above the melting temperature.[38] Unfortunately, the corresponding MS signals for these species could not be detected, since the relevant mass to charge ratio (m/e) exceeds the detection limit of the MS in this setup. However, within the same temperature range, an increase of almost 1 order of magnitude in the Cl signal (m/e = 35) was found.

The TG curves for metallurgical grade silicon (Si-Ref) and unreacted contact mass (S0) (Figure 1d) show an initial mass loss of 1.35−2.5% below 100 °C, which is attributed to drying. For Si-Ref, a small, continuous mass gain owing to silicon oxidation across the whole temperature range is thereafter noticed, in agreement with previous reports.[30] The unreacted contact mass (S0), however, experiences a continuous mass loss after 100 °C, which becomes sharper at around 422 °C. The observed mass changes in this sample may therefore result from a combination of an increase, due to silicon oxidation, and a decrease related to CuCl oxidation and decomposition.

The SEM image representative of the S0 sample and its corresponding elemental mapping illustrate the distribution of smaller CuCl particles over a larger silicon particle (Figure 1e)), and it is representative of the morphology of an unreacted contact mass.

3.2. Catalytic Performance. Si consumption, reactivity, and selectivity data, measured in the fluidized bed reactor, are shown in Figure 2. It is immediately noticeable that the relative amount of CuCl and the presence of Zn affect the silicon consumption. Si consumption increases steadily up to ∼10% through 5 h and further to ∼40% after 16 h when the standard amount of catalyst is used (i.e., S1−S4), whereas the consumption is substantially higher in 5 × Cu samples (i.e., S5−S8), consuming ∼80% of the Si within 16 h (Figure 2a-b). Increasing the catalyst + promoter/silicon ratio hence considerably accelerates the reactivity. The reactivity (Figure 2c-d) displays the rate of MCS (mass of gaseous products, M*i*) product formation relative to unconverted mass of Si in the reactor. We observe a strong increase within the first 5 h to 30−40% and 10−20% Si consumption for the 5 × Cu and std-Cu samples, respectively. Thereafter, a strong decline in reactivity for the 5 × Cu samples occurs before leveling off at a

https://doi.org/10.1021/acs.iecr.3c02940
Ind. Eng. Chem. Res. 2023, 62, 21579−21589

somewhat higher level than the std-Cu counterparts. The std-Cu contact masses exhibit neither the same high reactivity nor the decline within the reaction time of 16 h.

The overall trend in selectivity toward dimethyldichlorosilane only shows minor variation with relative amounts of CuCl; however, the maximum M2 selectivity is reached faster with the std-Cu samples (Figure 2e-f). After an induction period of ~2 h, 83−93% selectivity to M2 can be observed until it declines at high Si consumption. The gaseous product distributions for all contact mass samples are given in Figure 3. The main side products are M1 and MH, produced with higher selectivity than M2 during the first 20 min of reaction. M1 and MH selectivity increases again at the time where the M2 selectivity is declining. Other silane byproducts constitute only minor contributions to the products. The peak in M2 selectivity is more prominent in contact masses with 5 × Cu, compared to that in std-Cu samples. The selectivity to M3 ($(CH_3)_3SiCl$) also appears slightly lower for the 5 × Cu runs.

With respect to Zn promotion, the activity trends are clearer for 5 × Cu samples; the Si consumption and reactivity are higher in the Zn-promoted samples (S5 and S7) than those without Zn (S6 and S8) at the initial stage of the reaction (Figure 2a-d). This is also observed with std-Cu samples, but the difference is smaller (S1−S4). Zn-promoted contact masses show slightly, but consistently, higher M2 selectivity during the initial period than their counterparts without Zn, and the selectivity levels off at a slightly higher value (Figure 2e-f). However, M2 selectivity gradually decreases after ~30% of Si consumption with Zn-promotion, while it remains steady to higher Si consumption in samples without Zn (Figure 2b and f). Notably also, an earlier decline in reactivity with Zn present appears accompanied by a decrease in M2 selectivity.

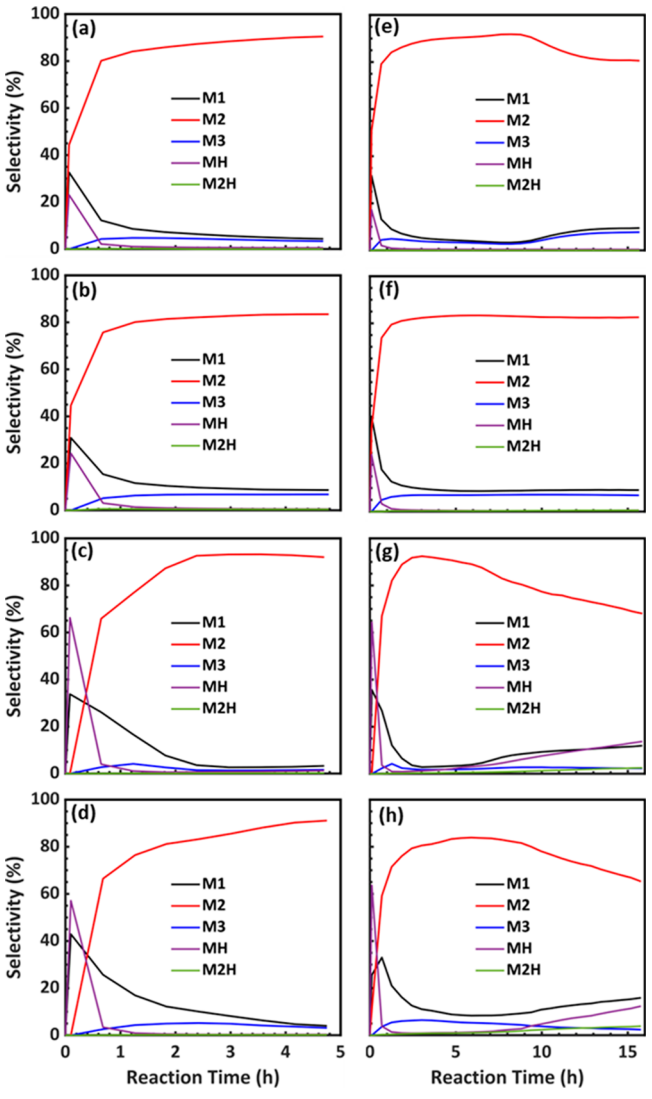

Figure 3. Product distribution over 5 h (a-d: left) and 16 h (e-h, right) MCS reaction times for all contact mass samples at 300 °C. The standard amount of the CuCl catalyst was added in the top four (a: S1, b: S2, e: S3, f: S4), and an increased (5×) amount of the CuCl catalyst was added in the lower four (c: S5, d: S6, g: S7, h: S8). S1, 3, 5, 7 (a, c, e, g) are Zn promoted; S2, 4, 6, 8 (b, d, f, h) have no Zn (all samples Sn promoted). M1: CH_3SiCl_3, M2: $(CH_3)_2SiCl_2$, M3: $(CH_3)_3SiCl$, MH: CH_3SiCl_2, M2H: $(CH_3)_2SiCl$, $(CH_3)_3Si_2Cl_3$, and $(CH_3)_4Si_2Cl_2$.

3.3. Characterization of the Reacted Contact Mass Samples. Figure 4 shows representative X-ray diffractograms of the postreaction contact mass samples with 5 and 16 h of reaction time. The XRD characteristic peaks for silicon already discussed in Section 3.1 are present in each sample (2θ of 28.5°, 47.3°, 56.1°, 69.1°, and 76.4°). The peaks at 2θ values of 43.3°, 50.4°, and 74.1° belong to metallic copper ; those at 44.5° and 45.1° represent the Cu_3Si, η-phase, and $Cu_{15}Si_4$ can be identified at 2θ values of 43.7° and 45.7°. The std-Cu contact masses (S1−S4) show little indication of different Cu species due to too low concentration. Clear fingerprints of metallic Cu, $Cu_{15}Si_4$, and Cu_3Si in the full 2θ region can only be detected for an increased Cu/Si ratio (S5−S8). Also the

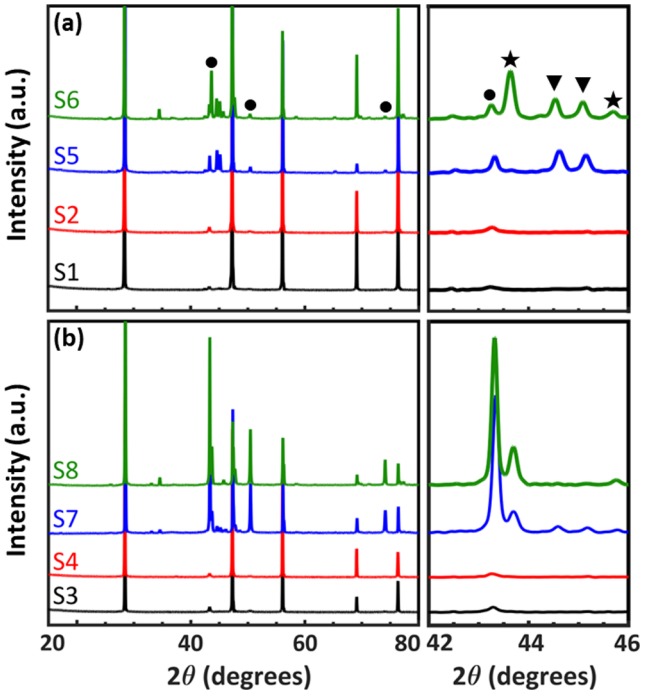

Figure 4. XRD pattern for contact mass samples after (a) 5 h and (b) 16 h of MCS reaction time with details of the 42°−46° region displayed to the left. The ●, ★, and ▼ symbols indicate metallic Cu (ICDD PDF#00-004-0836), $Cu_{15}Si_4$ (ICDD PDF#04-014-4307), and Cu_3Si (ICDD PDF#00-059-0262), respectively. S1−4: std-Cu; S5−8: 5 × Cu; S1, 3, 5, 7: Zn promoted; S2, 4, 6, 8: no Zn (all samples Sn promoted).

https://doi.org/10.1021/acs.iecr.3c02940
Ind. Eng. Chem. Res. 2023, 62, 21579−21589

weak CuCl peak at 33.0° is not discernible with the std-Cu amount (S1−S4), while it is visible in 5 × Cu samples (S5−S8), indicating that elevated amounts of CuCl at the start of the reaction either render it unreacted or induce its formation.

Cu^0, $Cu_{15}Si_4$, and Cu_3Si exhibit distinct peaks in the 42°−46° range of the XRD diagrams (zoom, Figure 4) that can be used for qualitative analysis of the development of the phases. The characteristic signal for metallic Cu (denoted as ●) increases substantially over the reaction time, i.e., from 5 to 16 h in samples with 5 × Cu (S5−S10), while the observable changes in samples with std-Cu (S1−S4) are marginal. The characteristic peaks related to Cu_3Si (denoted as ▼) and $Cu_{15}Si_4$ (denoted as ★) phases are also hardly visible in the samples with std-Cu, both with Zn (i.e., S1, S3) and without Zn present (i.e., S2, S4). This could be the result of continuous formation and consumption of these phases during the reaction.[39] However, these signals are clearly visible in samples with 5 × Cu, which makes it possible to discern the role of Zn. The signal intensity for the Cu_3Si phase is relatively more pronounced in samples with Zn than without. Moreover, the characteristic signals for $Cu_{15}Si_4$ show lower intensity and appear at longer reaction times in the Zn-promoted contact mass (i.e., S5, S7) than without Zn (i.e., S6, S8).

The SEM images shown in Figure 5 are examples, selected to represent the most typical surface morphology observations in these heterogeneous contact mass samples. There is a general difficulty in acquiring representative, high-resolution SEM images due to the roughness and heterogeneous nature of these samples that increase with exposure time. Systematic trends are therefore difficult to identify, especially for contact masses with low amounts of catalyst and promoter (std-Cu). We have therefore only included SEM images from samples with 5 × Cu and 5 h (samples S5 and S6). Figure 5 illustrates how the Si particle surface has been etched over the course of the reaction, with silicon consumption causing the formation of reaction pits. The surface morphology appears somewhat different between samples with Zn (S5, Figure 5a-b) and without Zn (S6, Figure 5c-d), since the etched region of S5 is covered by cube-shaped structures and flakes.

Corresponding elemental mapping and EDX spectra are shown in Figure 6. The cube-shaped structure in the Zn-promoted contact mass (S5) mainly contains Cu, and Cu and Zn are (generally) associated with each other (Figure 6a).

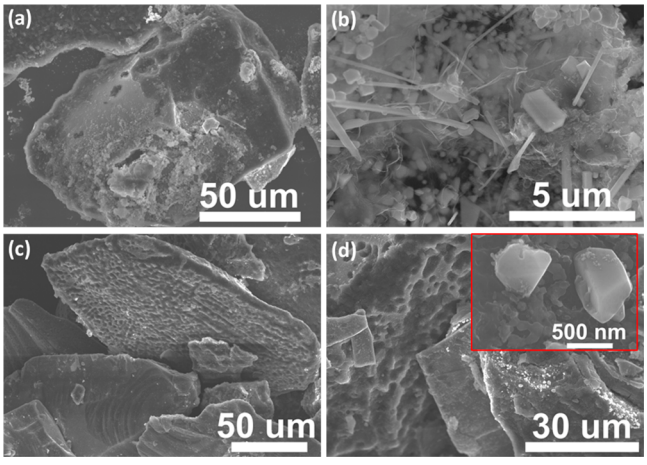

Figure 5. SEM images of 5 × Cu contact mass samples reacted for 5 h, (a,b) with Zn (S5) and (c,d) without Zn (S6) promotion.

Without Zn (S6), however, the Si surface tends to be covered by CuCl species (Figure 6b). Elemental mapping also generally suggests that the presence of carbon is linked to the location of copper on contact mass samples (several images and different exposures, not shown).

Raman spectra of the reacted contact mass samples are plotted in Figure 7. The bands at around 1150, 1310, and 1600 cm^{-1} are all attributed to carbonaceous species.[40] 1150 cm^{-1} is mainly assigned to C−H vibrations in hydrogenated coke.[41,42] 1310 cm^{-1} is known as the disordered (D) band, which is a characteristic feature of amorphous carbon.[43,44] 1600 cm^{-1} is known as the graphitic (G) band and representative of highly ordered, crystalline graphite.[44] The characteristic bands for carbonaceous species are less prominent in the 5 h samples (Figure 7a), but they are clearly visible after 16 h of MCS reaction time (Figure 7b). The spectral intensities are insufficient to show overtones (2D, ∼2660 cm^{-1}), but this could also signify little or no graphitization. The intensity of the G-band relative to the D-band appears to increase over time, suggesting less hydrogenated and more structurally ordered carbon as the reaction progresses. The std-Cu (S1−S4) samples also display smaller contributions in the carbonaceous species range than their 5 × Cu counterparts (S5−S8).

The effect of Zn promotion is not apparent directly from Raman spectra, but the intensity of the G-band also appears more prominent in samples with Zn (Figure 7, S3, S5, S7). The full width at half-maximum of the G-band ($fwhm_G$) computed for the contact mass samples after 16 h of reaction time (Table 2) suggests a narrower G-band (as calculated with Spectragryph - optical spectroscopy software version 1.1) and hence formation of more ordered carbon with Zn present.[45]

Figure 8 presents the DRIFTS spectra of reacted contact mass samples to yield surface chemical features. The band near 830 cm^{-1} is assigned to the deformation mode of surface (S) adsorbed H, δ(S−H), and its presence indicates the decomposition of CH_3 on the contact mass surface.[46] No significant difference is observed for this absorbance band between samples with and without Zn. The band is, however, more noticeable throughout the reaction, i.e., after 16 h (Figure 8), suggesting a higher concentration of H at the surface over the course of the reaction. The spectral regions around 900−1100 cm^{-1} and 1200−1500 cm^{-1} are dominated by the absorbances that we attribute to silicon−oxygen vibrations and C−H bending modes, respectively.[46,47] Again, no noticeable difference is observed for these bands other than that they are more visible as the reaction progressed in time. The band near 1600 cm^{-1} is due to stretching vibrations of carbon π-bonds (given as ν(C═C)).[48,49] It is detected mainly for 5 × Cu samples reacted for 16 h (S7−S8) but with higher intensity for the Zn promoted sample (S7). The bands found in the O−H stretching area (3200−3500 cm^{-1}) are most likely due to the presence of water in these samples,[47] taken up from air post MCS reaction, which is also supported by the TGA/MS results discussed below.

Very low amounts of carbon relative to total sample mass are present after 5 h of MCS reaction time. Systematic TGA and DSC trends were therefore more prominent and interpretable for the contact mass samples after 16 h (S3−S4 and S7−S8), and these are presented in Figure 9 together with MS signals for the evolved gases. All samples experience a mass loss of 1−2% below 100 °C, which is attributed to drying, aswell as dehydration of Si−OH groups present in the spent contact

https://doi.org/10.1021/acs.iecr.3c02940
Ind. Eng. Chem. Res. 2023, 62, 21579−21589

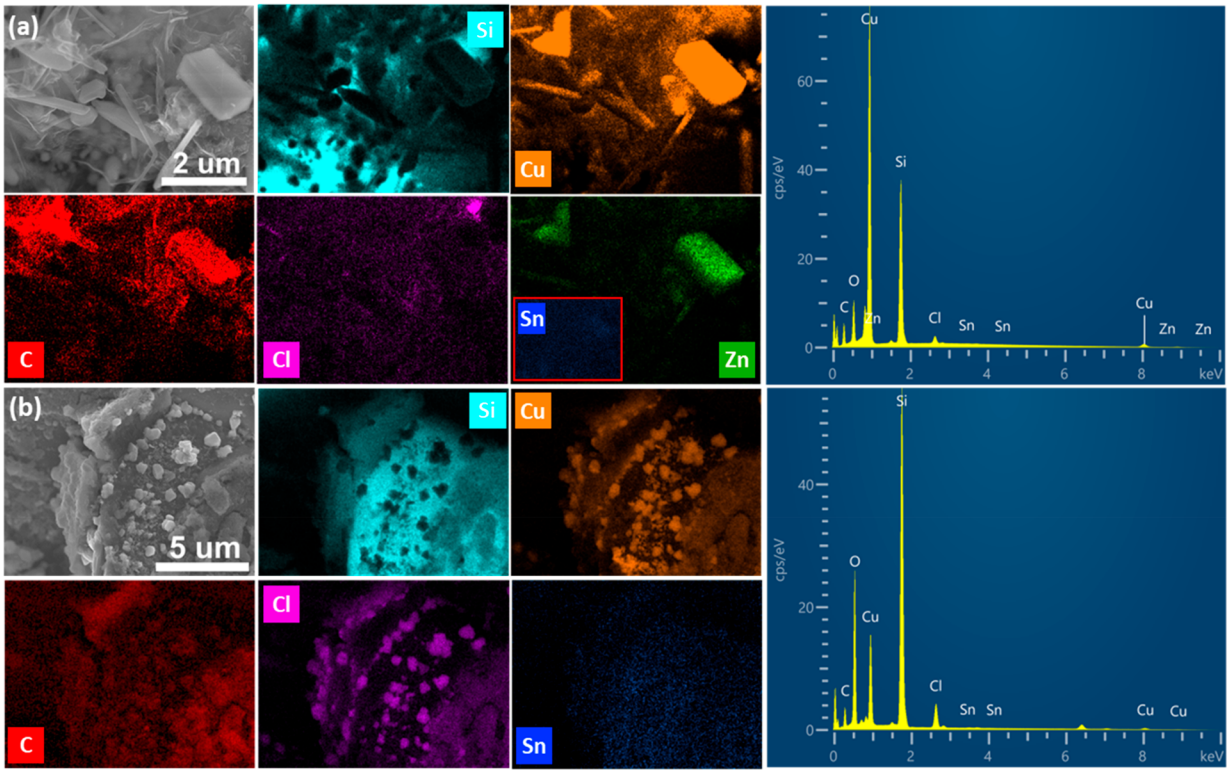

Figure 6. EDX elemental mapping and spectra of 5 × Cu contact mass samples reacted for 5 h, (a) with Zn (S5) and (b) without Zn (S6) promotion.

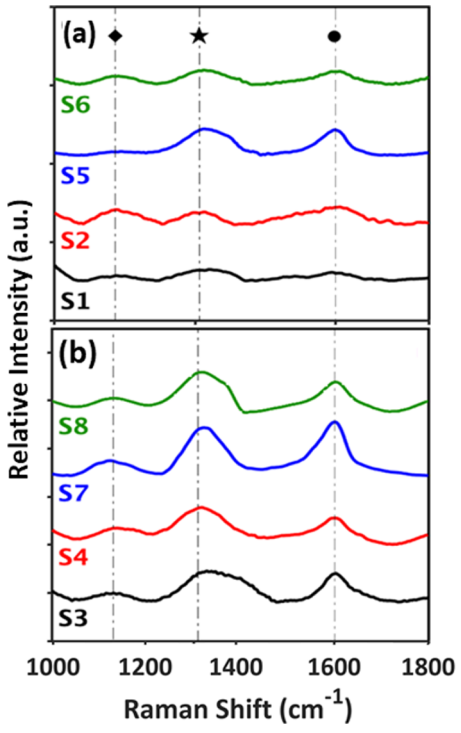

Figure 7. Raman spectra of contact mass samples, averaged over 5−10 points on each sample but not normalized, after (a) 5 h and (b) 16 h (c) of MCS reaction. ◆ denotes C−H vibrations (~1120 cm^{-1}), ★ D-band (~1310 cm^{-1}), and ● G-band (~1600 cm^{-1}). S1−4: std-Cu; S5−8: 5 × Cu; S1, 3, 5, 7: Zn promoted; S2, 4, 6, 8: no Zn (all samples Sn promoted).

Table 2. Calculated Full Width at Half Maximum of the G-Band ($FWHM_G$) for the Reacted Contact Mass Samples after 16 h of Reaction Time

Samples/description	$fwhm_G$ (cm^{-1})
S3 − 97.5%Si2.5%CuZnSn−16 h	60
S4 − 97.5%Si12.5%CuSn−16 h	91
S7 − 87.5%Si12.5%CuZnSn−16 h	67
S8 − 87.5%Si12.5%CuSn−16 h	81

mass[50], evidenced by the presence of H_2O (m/z = 18) signals below 100 °C in the MS spectra (Figure 9). The std-Cu samples (S3 and S4) undergo a continuous mass loss over the whole temperature range, with an overall mass loss of around 2.5%, as evidenced by TGA analysis in Figure 9a−b. A slight mass increase is obtained, however, for the 5 × Cu samples between 200−420 °C (S7 and S8, TG plots in Figure 9c−d). This can be attributed to a combined effect of mass loss and gain due to decomposition of carbonaceous species evidenced by CO_2 signals (m/z = 44) from the MS spectra and oxidation of (primarily) copper species, respectively. Note the order of magnitude difference in MS signal intensity for 5 × Cu as compared to std-Cu, as well as the CO_2 formation from the 5 × Cu samples also correlating well with the DSC exotherms. The small variations in the DSC signal from the std-Cu samples are difficult to interpret due to the high relative Si content. The higher Si consumption for 5 × Cu samples after 16 h renders more Cu and carbonaceous species per sample mass, and the concentration and nature of Cu species present may also affect the efficacy of coke oxidation. It is thus difficult to quantify differences in carbon formation based on the TGA results, but the MS data agree qualitatively with the Raman and DRIFTS spectra on increased coke formation with a higher

https://doi.org/10.1021/acs.iecr.3c02940
Ind. Eng. Chem. Res. 2023, 62, 21579−21589

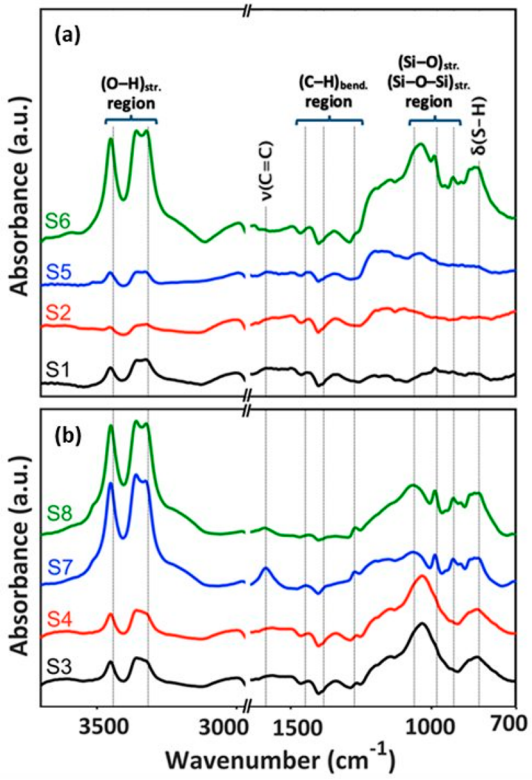

Figure 8. DRIFT spectra of contact mass samples after (a) 5 and (b) 16 h of MCS reaction. S1−4: std-Cu; S5−8: 5 × Cu; S1, 3, 5, 7: Zn promoted; S2, 4, 6, 8: no Zn (all samples Sn promoted).

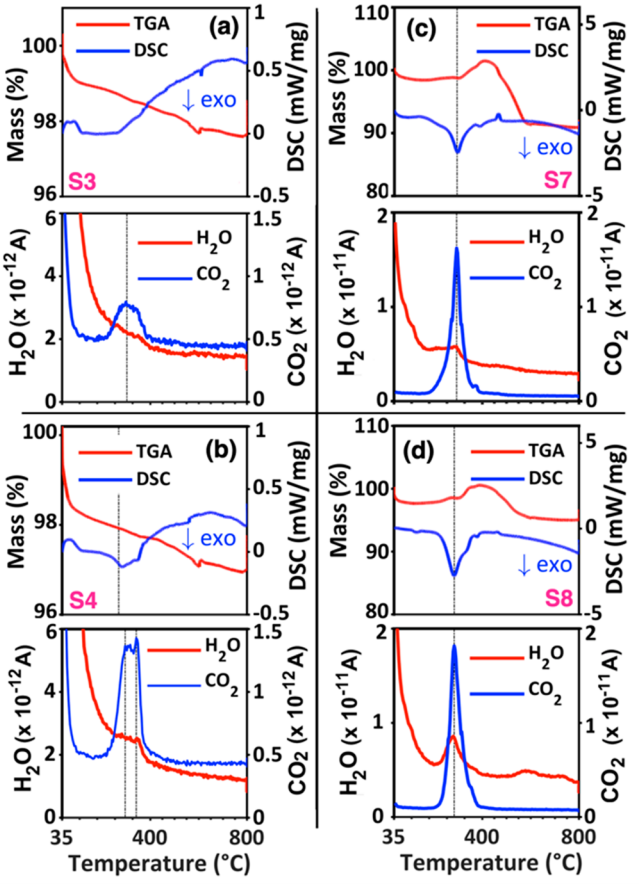

Figure 9. TGA, DSC, and MS profiles of the (a, b) std-Cu and (c, d) 5 × Cu contact mass samples (a, c; upper panels) with Zn and (b, d; lower panels) without Zn after 16 h of MCS reaction time. S3−4: std-Cu; S7−8: 5 × Cu; S3, S7: Zn promoted; S4, S8: no Zn (all samples Sn promoted).

Cu/Si ratio. A substantial mass loss is observed for these samples after 420 °C, likely associated with the decomposition/reaction of unreacted CuCl in the contact mass (Figure 1c).

The temperature profiles (Figure 9) of the MS spectra for CO_2 formation from the spent contact mass samples are summarized in Table 3. Coke oxidation is initiated at around 200 °C with a peak at around 300 °C. According to the literature, coke oxidized below 400 °C consists of amorphous structures, alkylated mono- and diaromatics, and surface and bulk carbide phases,[51,52] while coke oxidized above 400 °C is ascribed to polymeric carbon.[52] It appears that the amount of catalyst affects the nature and reactivity of the deposited coke because the CO_2 peak appears at lower temperatures in the 5 × Cu samples than in the std-Cu samples, and the oxidation of the coke is completed below 400 °C (Table 3). But, we speculate that high CuCl content increases the tendency of local hotspot formation during oxidation.[29] It is difficult to correlate MS CO_2 signal trends (and thus coke formation) with Zn promotion, but samples without Zn (S4 and S8) exhibit more prominent H_2O (m/z = 18) MS peaks at their respective peak temperatures of coke oxidation (Figures 9b, 9d) than their respective Zn-promoted counterparts (S3 and S7, Figures 9a and 9c). This is an indication that the deposited coke has higher hydrogen contents, which is in line with our findings from Raman spectroscopy (Figure 7).

Table 3. Temperature (°C) Profile of CO_2 (m/z = 44) MS Spectra for the Reacted Contact Mass Samples

Sample	Initial peak temp. (°C)	Main peak temp. (°C)	2nd peak temp. (°C)	End peak temp. (°C)
S1−97.5%Si2.5% CuZnSn−5 h	<200	336	-	440
S2−97.5%Si2.5% CuSn−5 h	<200	300	340	480
S3−97.5%Si2.5% CuZnSn−16 h	<200	300	-	440
S4−97.5%Si12.5% CuSn−16 h	<200	300	340	440
S5−87.5%Si12.5% CuZnSn−5 h	<200	276	-	400
S6−87.5%Si12.5% CuSn−5 h	<200	284	-	400
S7−87.5%Si12.5% CuZnSn−16 h	<200	287	375	400
S8−87.5%Si12.5% CuSn−16 h	<200	284	350	400

4. DISCUSSION

4.1. Methodology. The present work illustrates some of the challenges in studying the methylchlorosilane synthesis with high scientific accuracy. The presence of a solid reactant limits the precision of the reaction experiments and the possibility for extracting systematic data since there is no real steady-state, and it is difficult to ensure the absence of concentration and temperature gradients. The recent review by Zhang et al.[3] discusses how different catalysts and promoters in addition to the reactor design and process parameters influence the reaction rate and product distribution of the MCS process.

https://doi.org/10.1021/acs.iecr.3c02940
Ind. Eng. Chem. Res. 2023, 62, 21579−21589

The fluidized bed laboratory arrangement adopted in the present work has been developed by Elkem over decades and has demonstrated good reproducibility and capability with respect to extracting valuable insights.[53−55] In the present work, the protocol was extended to disentangle the effects of the reaction time and Cu/Si ratio in conjunction with the effect of the Zn promoter. In addition, we found that contact mass samples may change under exposure to ambient conditions. In order to extract good characterization data, storage under inert conditions must be ensured. Detailed mechanistic insight remains difficult, however, and thus, more theoretical approaches and use of model systems may prove highly useful.[56]

Our results confirm the heterogeneity of reacted contact masses, displaying unreacted Si with localized etching and differences in the CuCl, metallic Cu, and copper silicide phases as well as carbon of varying order, H-content, and reactivity. The somewhat similar reactivity and Si consumption between the std-Cu experiments after 16 h and 5 × Cu after 5 h suggest that higher Cu loadings may be used as representative, accelerated protocols for enhancing effects of a progressed reaction. A range of characterization tools was applied, each with−admittedly−limited precision due to the heterogeneity. This makes interpretations based on a single technique less conclusive, and thus, we made an effort to support our claims below with more than one result. The general challenge remains, however, to quantify both carbon formation and active species under controlled conditions.

4.2. Effect of Relative CuCl Contents on Catalytic Performances. In the MCS process, the interaction between Si and CuCl is a complex reaction system, whereby the active phase, Cu_3Si, is also formed. The equations below describe how Cu_3Si may form under reaction conditions (eq 4) and how excess CuCl may facilitate the transformation of the most active phase toward more copper-rich phases (e.g., $Cu_{15}Si_4$ and Cu_5Si) and ultimately metallic Cu (eqs 5−7).[57,58]

$$7Si_{(s)} + 12CuCl_{(s,g)} \rightarrow 4Cu_3Si_{(s)} + 3SiCl_{4(g)} \quad (4)$$

$$31Cu_3Si_{(s)} + 12CuCl_{(s,g)} \rightarrow 7Cu_{15}Si_{4(s)} + 3SiCl_{4(g)} \quad (5)$$

$$9Cu_{15}Si_{4(s)} + 20CuCl_{(s,g)} \rightarrow 31Cu_5Si_{(s)} + 5SiCl_{4(g)} \quad (6)$$

$$Cu_5Si_{(s)} + 4CuCl_{(s,g)} \rightarrow 9Cu_{(s)} + SiCl_{4(g)} \quad (7)$$

The Cu/Si ratio in the startup mass has a significant effect on the reactivity of the MCS process, and as shown in Figure 2, samples with 5 × Cu yield substantially higher Si consumption compared with the std-Cu samples. However, the initial increase in Si consumption/reactivity is not fully proportionate to the increased quantity of CuCl, and excess CuCl is also clearly associated with a decline in reactivity as the reaction progresses. Furthermore, higher CuCl concentration (5 × Cu) has no certain effect on the maximum selectivity compared to the std-Cu samples but results in a slightly longer induction period in the selectivity toward M2. The latter is difficult to explain and may suggest that parallel, or even reversible, reactions exist beyond eqs 4−7 above, affected by the initial CuCl concentration. Our XRD results demonstrate higher $Cu_{15}Si_4$ phase formation and Cu^0 enrichment in 5 × Cu samples over the reaction time (Figure 3). Jointly, this agrees well with the sequential scheme (eqs 5−7) of Weber et al.,[57] whereby the Cu_3Si phase can progressively be consumed by excess CuCl. Cu^0 is inactive toward MCS formation and facilitates the cracking of CH_3Cl,[59] leading to higher coke formation in 5 × Cu samples, as also evidenced by our Raman (Figure 7) and TGA/MS analyses (Figure 9).

4.3. Effect of Zn Contents on Catalytic Performances. Zn, as discussed initially, is added in parts per million quantities as a promoter for the MCS reaction. The Zn promoted samples here demonstrate a higher initial Si consumption and higher reactivity than that of samples without Zn. The sharper rise in the reactivity curve during the first 5 h (Figure 2c-d) indicates that Zn in low quantities promotes the active phase formation.[60] This is in agreement with the XRD analysis (Figure 4), where samples promoted with Zn display relatively higher signal intensities for Cu_3Si and lower intensities for $Cu_{15}Si_4$ phases, as also proposed by Agarwala et al.[14] In the absence of Zn, more copper-rich phases, i.e., $Cu_{15}Si_4$, and metallic copper, are formed. Formation of flakes and cube shaped structures where Cu and Zn are associated, observed via SEM and elemental mapping analyses (Figures 4 and 5), also suggests the role of Zn to be dispersing Cu and promoting the active phase formation.[61]

Zn-containing samples attain maximum reactivity and M2 selectivity sooner than their unpromoted counterparts. However, both drop earlier in these samples, while in the samples without Zn, even though the maximum M2 selectivity may be lower, it remains until more Si in the reactor is consumed. This can possibly be attributed to different cracking mechanisms and nature of deposited coke, since Zn also seems to promote higher structural order of the deposited coke, as shown by Raman spectroscopy (Figure 7) and thermogravimetric analyses (Figure 9). It has been reported that Zn may promote conversion of carbidic carbon into the graphitic carbon, thereby to some extent, intermittently "freeing" active sites for the reaction.[21,62] This is consistent with our findings from Raman spectroscopy, DRIFTS and TGA/MS/DSC, which indicate more C−C and lower C−H bond formation with Zn present. Finally, it should be kept in mind that all samples also contained Sn, and the effects of Zn promotion cannot be considered to be independent of the synergy with Sn.

5. CONCLUSION

The effects of the Cu/Si ratio and Zn promoter on the catalytic performance of the direct synthesis of methylchlorosilanes (MCS) have been investigated using contact mass samples with different Cu/Si ratios and reaction times. Formation of coke and the evolution of the Cu_xSi_y phase over reaction time have been studied using a variety of (postreaction) characterization techniques and correlated to fluidized bed lab-scale reactor MCS reaction data obtained in a semibatch mode, i.e. continuous flow of CH_3Cl but neither continuous nor periodic injection of Si.

A higher CuCl (5 × Cu) content significantly promotes silicon consumption and initial reactivity. However, higher $Cu_{15}Si_4$ phase formation and inactive Cu^0 enrichment in 5 × Cu samples over the reaction time are also found, which eventually leads to moderated reactivity as well as higher carbon formation than for the standard Cu/Si ratio. It could also be that the content of CuCl influences the nature and reactivity of the deposited coke. The dimethyldichlorosilane (M2) selectivity is not greatly affected by additional CuCl, but

https://doi.org/10.1021/acs.iecr.3c02940
Ind. Eng. Chem. Res. 2023, 62, 21579−21589

a slightly longer induction period in selectivity toward M2 is obtained.

It is found that Zn changes the etching mechanism of the Si particles and facilitates the formation of the active catalytic phase. This results in a shorter induction period, in which Zn-promoted samples attain maximum M2 selectivity and reactivity earlier than their unpromoted counterparts. The deposited carbon is generally reactive and amorphous in nature, but Zn appears to promote the structural order of the deposited coke and reduce its hydrogen content.

AUTHOR INFORMATION

Corresponding Author

Hilde J. Venvik − *Department of Chemical Engineering, NTNU - Norwegian University of Science and Technology, 7491 Trondheim, Norway;* orcid.org/0000-0002-8113-032X; Email: hilde.j.venvik@ntnu.no

Authors

Mehdi Mahmoodinia − *Department of Chemical Engineering, NTNU - Norwegian University of Science and Technology, 7491 Trondheim, Norway;* orcid.org/0000-0002-8450-9503

Hammad Farooq − *Department of Chemical Engineering, NTNU - Norwegian University of Science and Technology, 7491 Trondheim, Norway;* orcid.org/0000-0003-0570-7868

Torbjørn Røe − *Elkem Silicon Products, 7038 Trondheim, Norway*

Ingeborg-Helene Svenum − *Department of Chemical Engineering, NTNU - Norwegian University of Science and Technology, 7491 Trondheim, Norway; SINTEF Industry, 7465 Trondheim, Norway*

Complete contact information is available at: https://pubs.acs.org/10.1021/acs.iecr.3c02940

Notes

The authors declare no competing financial interest.

ACKNOWLEDGMENTS

This work was carried out as part of the project HECSI (High Efficiency Silicon for the silicone value chain 295861). The authors acknowledge the financial support from the Research Council of Norway via both the User-driven Research based Innovation BIA program, SkatteFUNN, the iCSI Centre for Researched-based Innovation (237922), and the Norwegian Micro- and Nano-Fabrication Facility, NorFab (295864).

REFERENCES

(1) Zhang, Y.; Li, J.; Liu, H.; Ji, Y.; Zhong, Z.; Su, F. Recent Advances in Rochow-Müller Process Research: Driving to Molecular Catalysis and to A More Sustainable Silicone Industry. *ChemCatChem.* **2019**, *11* (12), 2757−2779.

(2) Rochow, E. G. *An Introduction Chemistry of the Silicones*; John Wiley and Sons, Inc.: New York, 1946.

(3) Zhang, P.; Zhang, D.; Dong, J.; Chen, G.; Li, J. Direct Synthesis of Methylchlorosilanes: Catalysts, Mechanisms, Reaction Conditions, and Reactor Designs. *Org. Process Res. Dev.* **2022**, *26* (8), 2270−2280.

(4) Luo, W.; Zhang, G.; Wang, G.; Wang, J. Effect of Copper Content on the Direct Process of Organosilane Synthesis from Silicon and Methyl Chloride. *Tsinghua Sci. Technol.* **2006**, *11* (2), 252−258.

(5) Chen, X.; Jia, L.; Wang, Y.; Song, L.; Zhu, Y.; Liu, W.; Zhong, Z.; Su, F. Solvothermal Synthesis of Copper (I) Chloride Microcrystals with Different Morphologies as Copper-Based Catalysts for Dimethyldichlorosilane Synthesis. *J. Colloid Interface Sci.* **2013**, *404*, 16−23.

(6) Liu, H.; Li, J.; Ji, Y.; Zhang, Z.; Wang, X.; Zhong, Z.; Su, F. Diffusion-Controlled Synthesis of Cu-Based Catalysts for the Rochow Reaction. *Sci. China Mater.* **2017**, *60* (12), 1215−1226.

(7) Zhang, Y.; Li, J.; Liu, H.; Ji, Y.; Zhong, Z.; Su, F. Promoting Effect of In_2O_3 on CuO for the Rochow Reaction: The Formation of P-N Junctions at the Hetero-Interfaces. *J. Catal.* **2017**, *348*, 110−124.

(8) Bažant, V. On the Mechanism of the Direct Synthesis of Organohalogenosilanes. *Pure Appl. Chem.* **1969**, *19* (3−4), 473−488.

(9) Li, J.; Zhang, Z.; Ji, Y.; Jin, Z.; Zou, S.; Zhong, Z.; Su, F. One-Dimensional Cu-Based Catalysts with Layered Cu-Cu_2O-CuO Walls for the Rochow Reaction. *Nano Res.* **2016**, *9* (5), 1377−1392.

(10) Gilliam, W. F.; Schenectady, N. Y. Preparation of Dialkyl-Substituted Dihalogenosilanes. US2464033A, March 8, 1949.

(11) Lewis, K. M.; McLeod, D.; Kanner, B.; Falconer, J. L.; Frank, T. Surface-Chemical Studies of the Mechanism of the Direct Synthesis of Methylchlorosilanes. In *Catalyzed Direct Reactions of Silicon*; Lewis, K. M., Rethwisch, D. G., Eds.; Elsevier Science Ltd.: Amsterdam, 1993; pp 333−440.

(12) Sun, D.-H.; Bent, B. E.; Wright, A. P.; Naasz, B. M. Chemistry of the Direct Synthesis of Methylchlorosilanes. UHV Study of the Chemisorbed Fragments Methyl and Chlorine on Copper Silicide and Their Desorption Pathways. *J. Mol. Catal. A Chem.* **1998**, *131* (1), 169−183.

(13) Van Loo, F. J. J.; Vosters, P. J. C.; Becht, J. G. M.; Metselaar, R. The Influence of Impurities of the Kinetics and Morphology of Reaction Layers in Diffusion Couples. *Mater. Sci. Forum* **1988**, *29*, 261−274.

(14) Agarwala, J. P.; Falconer, J. L. Kinetics of Methylchlorosilane Formation on Zn-Promoted Cu_3Si. *Int. J. Chem. Kinet.* **1987**, *19* (6), 519−537.

(15) Halm, R. L.; Wilding, O. K., Jr.; Zapp, R. H. Method of Manufacturing Alkylhalosilanes. 4602101, July 22, 1986.

(16) Voorhoeve, R. J. H. *Organohalosilanes: Precursors to Silicones*; Elsevier Publishing Company: New York, 1967.

(17) Acker, J.; Köther, S.; Lewis, K. M.; Bohmhammel, K. The Reactivity in the System CuCl-Si Related to the Activation of Silicon in the Direct Synthesis. *Silicon Chem.* **2003**, *2* (3), 195−206.

(18) Rochow, E. G.; Gilliam, W. F. The Direct Synthesis of Phenylchlorosilanes. *J. Am. Chem. Soc.* **1945**, *67* (10), 1772−1774.

(19) Hurd, D. T.; Rochow, E. G. On the Mechanism of the Reaction between Methyl Chloride and Silicon-Copper. *J. Am. Chem. Soc.* **1945**, *67* (7), 1057−1059.

(20) Ballutaud, D.; de Mierry, P.; Aucouturier, M.; Darque-Ceretti, E. Influence of Thermal Treatments on the Distribution of Contaminating Copper near the Surface of Silicon: A Comparative SIMS and XPS Study. *Appl. Surf. Sci.* **1991**, *47* (1), 1−8.

(21) Frank, T. C.; Kester, K. B.; Falconer, J. L. Surface Analysis of Methylchlorosilane Formation Catalysts. *J. Catal.* **1985**, *95* (2), 396−405.

(22) Voorhoeve, R. J. H.; Lips, J. A.; Vlugter, J. C. Mechanism and Kinetics of the Metal-Catalyzed Synthesis of Methylchlorosilanes: I. The Synthesis of Methylchlorosilanes in a Fluid Bed. *J. Catal.* **1964**, *3* (5), 414−425.

(23) Bablin, J. M.; Lewis, L. N.; Bui, P.; Gardner, M. Mechanism of the Methylchlorosilane Reaction: Improved Lab Reactor Design and Kinetic Data. *Ind. Eng. Chem. Res.* **2003**, *42* (15), 3532−3543.

(24) Banholzer, W. F.; Lewis, N.; Ward, W. Active Site Formation in the Direct Process for Methylchlorosilanes. *J. Catal.* **1986**, *101* (2), 405−415.

(25) Kim, J. P.; Rethwisch, D. G. The Direct Synthesis of Methylchlorosilanes I. Steady-State and Transient Reaction Kinetics. *J. Catal.* **1992**, *134* (1), 168−178.

(26) Setínek, K.; Bažant, V.; Šorm, F. Organische Siliciumverbindungen XI. Stoffbilanz Der Direkten Synthese von Methylchlorsilanen. *Collect. Czech. Chem. Commun.* **1957**, *22* (4), 1192−1198.

(27) Bažant, V. Direct Synthesis of Organohalogenosilanes. *Pure Appl. Chem.* **1966**, *13* (1−2), 313−328.

(28) Blaser, E.; Rosier, C.; Huet, M.; Geantet, C.; Loridant, S. Catalytic Cracking of CH_3Cl on Copper-Based Phases. *Catal. Sci. Technol.* **2022**, *12* (6), 2006−2014.
(29) Clarke, M. P. The Direct Synthesis of Methylchlorosilanes. *J. Organomet. Chem.* **1989**, *376* (2), 165−222.
(30) Wessel, T. J.; Rethwisch, D. G. Deactivation of CuSi and CuZnSnSi Due to Coke Formation during the Direct Synthesis of Methylchlorosilanes. *J. Catal.* **1996**, *161* (2), 861−866.
(31) Jia, Z.; Zhang, C.; Cai, D.; Blair, E.; Qian, W.; Wei, F. The Analysis of Hot Spots in Large Scale Fluidized Bed Reactors. *RSC Adv.* **2017**, *7* (33), 20186−20191.
(32) Blaser, E.; Rosier, C.; Huet, M.; Chaurand, P.; Geantet, C.; Loridant, S. Thermal Cracking of CH_3Cl Leads to Auto-Catalysis of Deposited Coke. *Catal. Sci. Technol.* **2021**, *11* (2), 469−473.
(33) Wang, A.; Zhang, M.; Yin, H.; Liu, S.; Liu, M.; Hu, T. Direct Reaction between Silicon and Methanol over Cu-Based Catalysts: Investigation of Active Species and Regeneration of CuCl Catalyst. *RSC Adv.* **2018**, *8* (34), 19317−19325.
(34) Sun, X.; Zhang, X.; Cao, X.; Zhao, X. Optimization of Reaction Conditions for Cyclohexane to Cyclohexanone with *t*-Butylhydroperoxide Over $CuCl_2$ Loaded with Activated Carbon. *J. Braz. Chem. Soc.* **2015**, *27* (1), 202−208.
(35) Uchinokura, K.; Sekine, T.; Matsuura, E. Raman Scattering by Silicon. *Solid State Commun.* **1972**, *11* (1), 47−49.
(36) Deng, Y.; Handoko, A. D.; Du, Y.; Xi, S.; Yeo, B. S. In Situ Raman Spectroscopy of Copper and Copper Oxide Surfaces during Electrochemical Oxygen Evolution Reaction: Identification of CuIII Oxides as Catalytically Active Species. *ACS Catal.* **2016**, *6* (4), 2473−2481.
(37) De Micco, G.; Bohé, A. E.; Pasquevich, D. M. A Thermogravimetric Study of Copper Chlorination. *J. Alloys Compd.* **2007**, *437* (1), 351−359.
(38) Guido, M.; Balducci, G.; Gigli, G.; Spoliti, M. Mass Spectrometric Study of the Vaporization of Cuprous Chloride and the Dissociation Energy of Cu_3Cl_3, Cu_4Cl_4, and Cu_5Cl_5. *J. Chem. Phys.* **1971**, *55* (9), 4566−4572.
(39) Wang, C.; Liu, T.; Huang, Y.; Wang, G.; Wang, J. Promoter Effects of Zn and Sn in the Direct Synthesis of Methylchlorosilanes. *Ind. Eng. Chem. Res.* **2013**, *52* (15), 5282−5286.
(40) Tuinstra, F.; Koenig, J. L. Raman Spectrum of Graphite. *J. Chem. Phys.* **1970**, *53* (3), 1126−1130.
(41) Guichard, B.; Roy-Auberger, M.; Devers, E.; Rebours, B.; Quoineaud, A. A.; Digne, M. Characterization of Aged Hydrotreating Catalysts. Part I: Coke Depositions, Study on the Chemical Nature and Environment. *Appl. Catal. A: Gen.* **2009**, *367* (1), 1−8.
(42) Bare, S. R.; Vila, F. D.; Charochak, M. E.; Prabhakar, S.; Bradley, W. J.; Jaye, C.; Fischer, D. A.; Hayashi, S. T.; Bradley, S. A.; Rehr, J. J. Characterization of Coke on a Pt-Re/γ-Al_2O_3 Re-Forming Catalyst: Experimental and Theoretical Study. *ACS Catal.* **2017**, *7* (2), 1452−1461.
(43) Beny-Bassez, C.; Rouzaud, J. N. Characterization of Carbonaceous Materials by Correlated Electron and Optical Microscopy and Raman Microspectroscopy. *Scan. Electron Microsc.* **1985**, *1*, 119−132.
(44) Beyssac, O.; Goffé, B.; Chopin, C.; Rouzaud, J. N. Raman Spectra of Carbonaceous Material in Metasediments: A New Geothermometer. *J. Metamorph. Geol.* **2002**, *20* (9), 859−871.
(45) DiLeo, R. A.; Landi, B. J.; Raffaelle, R. P. Purity Assessment of Multiwalled Carbon Nanotubes by Raman Spectroscopy. *J. Appl. Phys.* **2007**, *101* (6), 064307.
(46) Gordon, A. D.; Hinch, B. J.; Strongin, D. R. Effects of Individual Promoters on the Direct Synthesis of Methylchlorosilanes. *J. Catal.* **2009**, *266* (2), 291−298.
(47) Rubio, F.; Rubio, J.; Oteo, J. L. A FT-IR Study of the Hydrolysis of Tetraethylorthosilicate (TEOS). *Spectrosc. Lett.* **1998**, *31* (1), 199−219.
(48) Savin, V. I.; Kitaev, Yu. P.; Saidashev, I. I. α,β-Unsaturated Carbonyl Compounds and Their Derivatives. Communication 1. Stereochemistry and IR Spectra of Aromatic α,β-Unsaturated Ketones. *Bull. Acad. Sci. USSR, Div. Chem. Sci.* **1972**, *21* (4), 807−812.
(49) Lim, M. H.; Blanford, C. F.; Stein, A. Synthesis and Characterization of a Reactive Vinyl-Functionalized MCM-41: Probing the Internal Pore Structure by a Bromination Reaction. *J. Am. Chem. Soc.* **1997**, *119* (17), 4090−4091.
(50) Wu, X.; Zhang, W.; Li, Z.; Zhang, Y.; Huang, S.; Liu, Q. Effects of Various Methylchlorosilanes on Physicochemical Properties of Ambient Pressure Dried Silica Aerogels. *J. Nanopart. Res.* **2019**, *21* (11), 234.
(51) Wolf, M.; Raman, N.; Taccardi, N.; Haumann, M.; Wasserscheid, P. Coke Formation during Propane Dehydrogenation over Ga-Rh Supported Catalytically Active Liquid Metal Solutions. *ChemCatChem.* **2020**, *12* (4), 1085−1094.
(52) Fei Tan, K.; Xu, J.; Chang, J.; Borgna, A.; Saeys, M. Carbon Deposition on Co Catalysts during Fischer−Tropsch Synthesis: A Computational and Experimental Study. *J. Catal.* **2010**, *274* (2), 121−129.
(53) Tysseland, A.; Vanhaecke, E. M. M.; Svenum, I.-H.; Blekkan, E. A.; Venvik, H. J. New Approaches to the Investigation of Carbon Formation in the Direct Synthesis of Methylchlorosilanes. In *Silicon for the Chemical and Solar Industry XIV, June 11−14, 2018, Svolvær, Norway*; Andresen, B., Nygaard, L., Rong, H. M., Tangstad, M., Tveit, H., Eds.; Norges teknisk-naturvitenskapelige universitet: Trondheim, Norway, 2018; pp 277−288.
(54) Mahmoodinia, M.; Bleken, F.; Svenum, I.-H.; Rø, T.; Blaser, E.; Gouttebroze, S.; Venvik, H. J. Role of Copper in the Formation of Carbon during Direct Synthesis of Methylchlorosilanes. In *Proceedings of the Silicon for the Chemical and Solar Industry XVI, June 14−16, 2022, Trondheim, Norway*; Tangstad, M., Rong, H. M., Walderhaug, Aa., Andresen, B., Tveit, H., Page, I. G., Eds.; Elsevier: Trondheim, Norway, 2022; DOI: 10.2139/ssrn.4118708.
(55) Brookes, K. H.; Siddiqui, M. R. H.; Rong, H. M.; Joyner, R. W.; Hutchings, G. J. Effect of Al and Ca Addition on the Copper Catalysed Formation of Silanes from Si and CH3Cl. *Applied Catalysis A: General* **2001**, *206* (2), 257−265.
(56) Svenum, I.-H.; Gouttebroze, S.; Bleken, F. L. Toward Understanding the Formation of Coke during the MCS Reaction: A Theoretical Approach. *J. Phys. Chem. C* **2023**, *127* (14), 6680−6689.
(57) Weber, G.; Viale, D.; Souha, H.; Gillot, B.; Barret, P. Kinetic Data and Mechanistic Model for the Reaction between Si and CuCl. *Solid State Ion.* **1989**, *32*−*33*, 250−257.
(58) Luo, W.; Wang, G.; Wang, J. Surface Morphology and Catalytic Activity of the Contact Mass in Organosilane Synthesis. *Chem. Eng. Commun.* **2006**, *193* (6), 754−763.
(59) Acker, J.; Bohmhammel, K. Thermodynamic Assessment of the Copper Catalyzed Direct Synthesis of Methylchlorosilanes. *J. Organomet. Chem.* **2008**, *693* (15), 2483−2493.
(60) Adonin, N. Yu.; Prikhod'ko, S. A.; Shabalin, A. Yu.; Prosvirin, I. P.; Zaikovskii, V. I.; Kochubey, D. I.; Zyuzin, D. A.; Parmon, V. N.; Monin, E. A.; Bykova, I. A.; Martynov, P. O.; Rusakov, S. L.; Storozhenko, P. A. The "Direct" Synthesis of Trialkoxysilanes: New Data for Understanding the Processes of the Copper-Containing Active Sites Formation during the Activation of the Initial Silicon Based Contact Mass. *J. Catal.* **2016**, *338*, 143−153.
(61) Gasper-Galvin, L. D.; Sevenich, D. M.; Friedrich, H. B.; Rethwisch, D. G. Role of Metallic Promoters in the Direct Synthesis of Methylchlorosilanes. *J. Catal.* **1991**, *128* (2), 468−478.
(62) Ehrich, H.; Born, D.; Richter, K.; Richter-Mendau, J.; Lieske, H. SEM-EDX and SAM-AES Investigations on Rochow Contact Masses. *Appl. Organomet. Chem.* **1997**, *11* (3), 237−247.